Small-Signal Analysis and Design of Constant On-Time Controlled Buck Converters With Duty-Cycle-Independent Quality Factors

Wen-Chin Liu, *Student Member, IEEE*, Ching-Hsiang Cheng, Patrick P. Mercier, *Senior Member, IEEE*, and Chunting Chris Mi, *Fellow, IEEE*

***Abstract*—This article presents a frequency-domain analysis that models the behavior of Constant-on-Time (COT)-controlled buck converters in wide-input–output-range scenarios. Based on this analysis, a design strategy is proposed to enable robust control with a duty-cycle-independent quality factor, also known as a constant Q-value. A constant Q-value circuit based on the proposed strategy is then constructed and incorporated with a baseline ultrafast transient COT control scheme to experimentally verify the system stability and optimal load transient response under wide input–output range scenarios. In addition, the design strategy is extended to other COT buck control schemes with simulation and calculation verifications.**

***Index Terms*—Constant Q-value, constant on-time (COT) control, ultrafast transient COT (UFTCOT) buck converter, wide-duty-cycle-range operation.**

I. Introduction

CONSTANT on-time (COT) controlled buck converters are widely used when powering central processing units (CPUs) and digital system-on-chips (SoCs) in consumer electronics applications, in part due to their ability to respond to rapid load current changes while also achieving high efficiency across a large dynamic range of load conditions. Typically, the input supply voltage—either from a battery or another power rail—is between 4 and 24 V, while the CPU and SoC loads generally require 0.5–3.3 V. A wide input-to-output voltage range requires a wide duty-cycle range in a COT-based buck converter controller, which can lead to concerns regarding stability, especially when a high bandwidth, rapid response-time design is desired.

Since the location of high-frequency complex poles in a COT system is usually a function of duty cycle [1], [2], [3], [4], [5], it is possible that duty-cycle variation can move these poles to the right-half plane (RHP), resulting in system instability. During stable operation, the duty cycle and the output voltage operate normally; however, in an unstable condition, the duty cycle shows a subharmonic oscillation, making the output voltage ripple significantly larger than in the stable condition. Due to the large potential dynamic range of duty cycle in consumer electronics applications, additional attention is thus required when designing a COT-controlled buck converter.

A wide input-to-output voltage range also presents increased challenges toward a high bandwidth COT design because, again, the location of poles, especially the high-frequency conjugate poles, are a function of duty cycle. For a pair of conjugate poles, the location can be represented by the frequency and the quality factor, Q, where the value of Q indicates the damping ratio of a system (i.e., $Q = \frac{1}{2\zeta}$), implying the poles' distance toward the real and the imaginary axis in the s-plane. Combining the abovementioned statements, Q is thus also a function of duty cycle because the poles, whose locations are highly related to duty cycle, can be partially represented by Q [1], [2], [3], [4], [5], [9].

A design example of an ultrafast transient COT (UFTCOT) control with simple type II compensation is shown in Fig. 1 to illustrate the challenges when Q varies due to changes in duty cycle. Under a low Q, low duty cycle, situation (the solid line), the complex poles split into two real poles, which move toward the low-frequency and the high-frequency regions, respectively. This can add some additional phase drop near the unity gain bandwidth, potentially presenting stability issues. On the other hand, in the high-Q, high duty cycle, situation (the dashed line), the gain at high frequencies may cross 0 dB twice for a high bandwidth design, as highlighted by the solid pink lines, resulting in instability. From this example, it should be clear that either a low or high Q can be detrimental to a system. Unfortunately, most COT-controlled buck converters suffer from the Q-value issue. Hence, to avoid this issue, a well-controlled and duty-cycle-independent Q-value is desired for a wide-duty-cycle-range operation in a COT controller.

Manuscript received 21 September 2022; revised 23 January 2023 and 7 April 2023; accepted 17 April 2023. Date of publication 20 April 2023; date of current version 19 May 2023. Recommended for publication by Associate Editor D. Maksimovic. *(Corresponding author: Chunting Chris Mi.)*

Wen-Chin Liu is with the Department of Electrical and Computer Engineering, University of California San Diego, La Jolla, CA 92093 USA, and also with the Department of Electrical and Computer Engineering, San Diego State University, San Diego, CA 92182 USA (e-mail: brianliu@eng.ucsd.edu).

Ching-Hsiang Cheng is with the Department of Electrical Engineering, National Taiwan University, Taipei 10617, Taiwan (e-mail: wind19871219@gmail.com).

Patrick P. Mercier is with the Department of Electrical and Computer Engineering, University of California San Diego, La Jolla, CA 92093 USA (e-mail: pmercier@ucsd.edu).

Chunting Chris Mi is with the Department of Electrical and Computer Engineering, San Diego State University, San Diego, CA 92182 USA (e-mail: mi@ieee.org).

Color versions of one or more figures in this article are available at https://doi.org/10.1109/TPEL.2023.3268613.

Digital Object Identifier 10.1109/TPEL.2023.3268613

TABLE I
LITERATURE REVIEW FOR COT-CONTROLLED BUCK CONVERTER IN A WIDE-RANGE OPERATION

Literature	Specific control	Implementation	Limitation
S. Bari et al. [5]	IQCOT	An adaptive threshold voltage proportional to the output voltage	Q-value variation is reduced but still vary with duty ratios. Load transient is not optimized.
K. Cheng et al. [6]	RBCOT	An internally adaptive ramp generated by high-pass filter	Enhanced stability and transient response but Q-value variation is not discussed.
T. Qian et al. [7]	RBCOT	An adaptive ramp achieved by off-time sensing	Only discussed stability issue, Q-value appears to vary with duty ratios.
W. Liu et al. [8]	RBCOT	An adaptive ramp controlled by input/output voltage and duty signal signal	Stability and transient response is improved but Q-value only nearly constant; namely, it still varies with duty ratios.
Y. Lin et al. [9]	RBCOT	A VIC ramp generated from low-pass filter	Q-value varies significantly over a wide-duty-cycle range to ensure stability an large ramp typically required, sacrificing transient performance.
K. Kong et al. [10]	RBCOT	An adaptive ramp generated by duty signal feedback and sample-and-hold circuit	A constant Q-value is achieved to improve both stability and transient response but the system exists low-frequency poles, limiting high-bandwidth design. Besides, the Q-value exists a minimum value, confining the design flexibility.

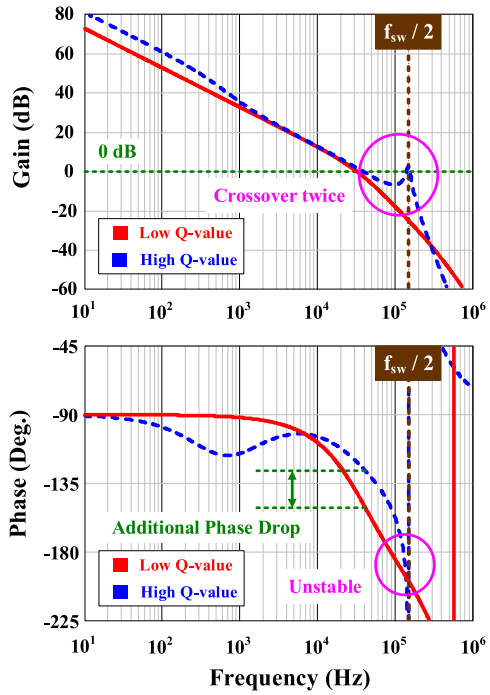

Fig. 1. High bandwidth design example.

In addition to stability and high bandwidth challenges, load transient performance is also affected by the wide-duty-cycle-range operation since the duty-cycle variation affects system behavior yet again. Specifically, the output impedance of a converter, which is often used to evaluate load transient response, also has a dependence on Q [1], [2]. As is well known in control theory, if a step response is applied to a high Q system, ringing can become significant, which is not desirable in a well-designed system. Thus, a high Q-value should be prevented under a wide-duty-cycle-range operation.

In summary, duty-cycle variation, as expected in many consumer electronics applications, poses significant challenges to stability, bandwidth, and response time, largely due to corresponding variations in Q. Unfortunately, most of the COT-controlled buck converters suffer from the exact same difficulties mentioned previously because the Q shows up at the half-switching frequency in the small-signal models. [2], [4], [5], [8], [9], [11], [12], [13]. Although [5], [6], [7], [8], [9], [10] reported different adaptive methods to reduce Q variation over the wide-duty-cycle-range operation, improving stability and transient response performance while alleviating difficulties in bandwidth design, as illustrated in Table I, most of them (e.g., [5], [6], [7], [8], [9]) cannot entirely remove the variation caused by the change of duty ratios. Although the method proposed in [10] can achieve an invariant Q-value, the developed system has a pair of low-frequency ($< f_{sw}/2$) conjugate poles, limiting high-bandwidth design. Besides, there is a lower limit for the Q-value design in [10], confining the design flexibility. Instead, a simple, well-controlled, and duty-cycle-independent Q-value, also known as constant Q-value, is desired for COT-controlled buck converters.

By analytically examining the small signal models, a generalized strategy to design a well-controlled and duty-cycle-independent quality factor for charged-based and ripple-based COT (RBCOT)-controlled buck converter with continuous ramp compensation is proposed in this article. Because of its excellent multiphase and load transient response performance, the UFTCOT [12] controller is taken as the baseline design to validate the proposed concept. Accordingly, a constant Q-value circuit compatible with the UFTCOT control scheme is proposed and designed. Finally, a PCB design for UFTCOT with a constant Q-value circuit is implemented, tested, and verified.

This article is organized as follows. The operation and small-signal models of UFTCOT control are demonstrated in Section II. In Section III, a general concept is proposed to

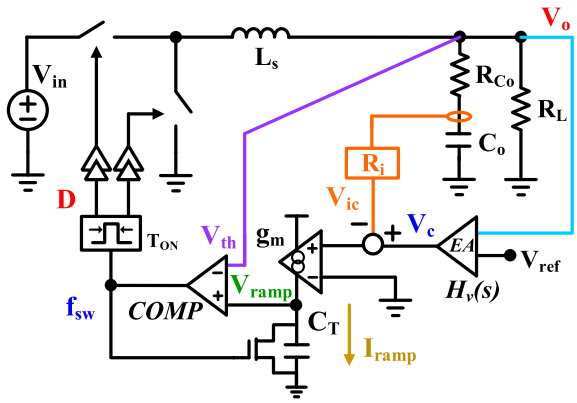

Fig. 2. Circuit diagram of the baseline UFTCOT control scheme for a buck converter.

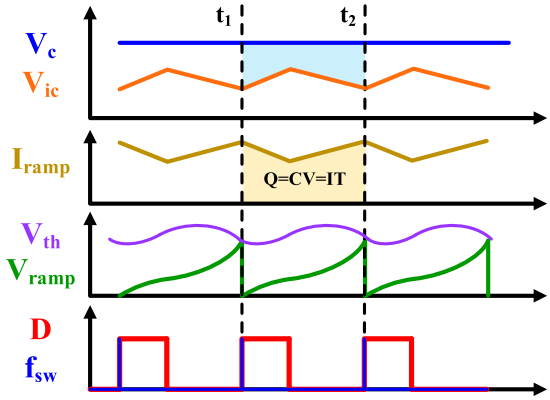

Fig. 3. Modulation waveforms of UFTCOT control scheme.

achieve a constant Q-value. Then, a constant Q-value circuit is presented for the UFTCOT control scheme. Next, the constant Q-value concept is extended to other existing control methods in Section IV. Finally, the simulation and experimental results are presented in Section V.

II. UFTCOT Control

The circuit diagram and modulation waveforms of the baseline UFTCOT-controlled buck converter [12] used in this work are shown in Figs. 2 and 3, respectively. During a cycle from T_1 to T_2, the output voltage is fed back to an error amplifier to calculate output regulation control voltage, V_c, forming an output voltage regulation feedback loop. Then, V_c is subtracted by a signal representing the current through the output decoupling capacitor, V_{ic}, which is converted to a voltage via resistor gain, R_i, in order to form a capacitor current feedback loop. The difference between V_c and V_{ic} is then sent to a voltage-to-current transconductor, converting the difference into a ramp current, I_{ramp}, to charge a threshold capacitor, C_T. As I_{ramp} charges C_T, the ramp voltage, V_{ramp}, on C_T starts to be built and is compared with the output threshold voltage, V_{th} through a comparator, COMP, where another threshold feedback loop is formed. Once V_{ramp} reaches V_{th}, a frequency signal, f_{sw}, is generated to trigger the on-time generator, T_{on}, for a fixed on-time duty signal, D, while activating the local feedback switch to purge the charge stored in C_T and start a new cycle. Note that the duty signal is set to be low automatically when its duration equals the on-time set by the on-time generator. Therefore, there are three global feedback loops as follows.

1) An output voltage feedback loop.
2) A capacitor current feedback loop.
3) An output voltage threshold loop, along with a local feedback loop to achieve modulation in this control scheme.

Here, the UFTCOT control scheme looks like the RBCOT with capacitor current compensation control scheme [14] at the very first glance since both of them take capacitor current and output voltage into their modulation; however, they are actually two different controls with very different modulation laws. The key difference is that the RBCOT with capacitor current compensation control is a ripple-based modulation control, and the UFTCOT control is a charge-based control. In the ripple-based controls, the modulation relies on the ripples of the output voltage and/or the compensated ramps, i.e., the inductor current and capacitor current; on the other hand, the charge-based control in UFTCOT uses the voltage difference between the control voltage, V_c, and sensed capacitor current, V_{ic}, that creates ramp current, I_{ramp}, to charge a threshold capacitor, C_T, generating an internal ramp, V_{ramp}, and then compares the ramp with the threshold voltage, V_{th}, to achieve its modulation. Therefore, charge-based control does not count on the ripple to achieve its modulation, and one of the charge-based control benefits is that no extra ramp compensation is required in multiphase operation, even when the system operates at ripple cancellation points [12]. The control-to-output transfer function, $G_{vc}(s)$, of UFTCOT can be derived using describing function (DF) analysis [15]. The result is shown in (1), where s_f is the sensed falling slope of the inductor current; R_i is the sensing gain; R_L is the load resistance; C_o is the output capacitance; R_{Co} is the equivalent series resistance (ESR); C_T is the threshold capacitor; V_{th} is the threshold voltage, which equals the output voltage in this case; g_m is the transconductance; and D denotes the duty cycle

$$\frac{\hat{v}_o(s)}{\hat{v}_c(s)} \approx K_c \frac{(R_{Co}C_o s+1)}{{}^{s}/_{\omega_a}+1} \frac{1}{1+\frac{s}{Q_1\omega_1}+\frac{s^2}{\omega_1^2}} \frac{1}{1+\frac{s}{Q_2\omega_2}+\frac{s^2}{\omega_2^2}} \tag{1}$$

where

$$K_c = \frac{R_L}{R_i\left(1-R_L\times k_2\right)}$$

$$\omega_a = \frac{1-R_L\times k_2}{\left(R_L+R_{C_o}\right)C_o - R_L R_{C_o} C_o \times k_2}$$

$$k_2 \approx -\frac{C_T}{g_m}\frac{2V_{\text{th}}}{V_{\text{in}}R_i T_{\text{on}}}+\frac{1}{R_L}$$

$$\omega_1 = {}^{\pi}/_{T_{\text{on}}} \qquad Q_1 = {}^{2}/_{\pi} \qquad \omega_2 = {}^{\pi}/_{T_{\text{sw}}}$$

$$Q_2 = \frac{T_{\text{sw}}}{\pi}\frac{1}{\left(\frac{C_T V_{\text{th}} D}{g_m T_{\text{on}} s_f}-\frac{T_{\text{on}}}{2}\right)} \qquad s_f = R_i\frac{V_o}{L_s}.$$

It can be seen that Q_2 at ω_2, which is equivalent to half the switching frequency, $f_{\text{sw}}/2$, is a function of the duty cycle. When

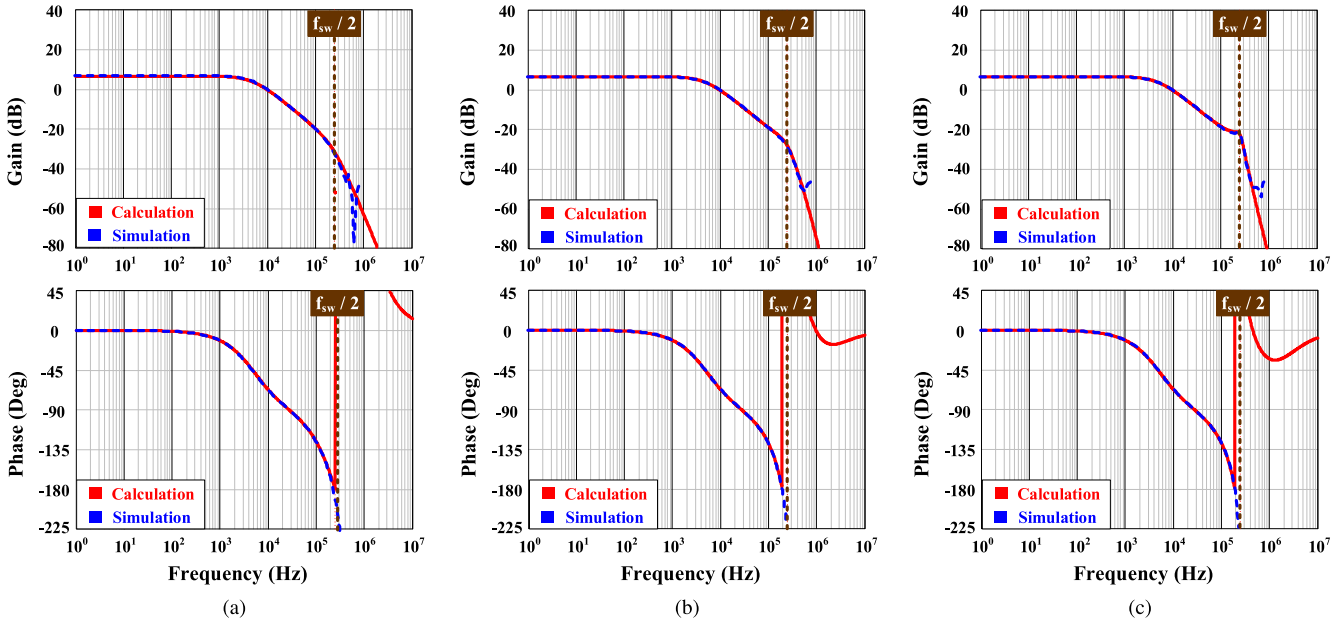

Fig. 4. Control-to-output transfer function validation. (a) D = 0.1, Q-value = 0.64. (b) D = 0.5, Q-value = 0.96. (c) D = 0.9, Q-value = 2.39.

the Q-value becomes a negative value, there are RHP poles appeared in $G_{vc}(s)$, causing system instability, and hence, the stability criteria can be found from Q_2 in (1), which can be expressed as (2). On the other hand, Q_1 at ω_1 is duty-cycle-independent and is thus not considered further

$$\frac{C_T L_s}{R_i g_m T_{\text{sw}}} > \frac{T_{\text{on}}}{2}. \tag{2}$$

It should note that the other COT-based control schemes [5], [6], [7], [8], [9], [10] also exhibit the similar behavior wherein Q_2 at ω_2 is a function of the duty ratio, potentially leading to stability issues. The effect of duty-ratio variation in Q_2 for other schemes will be illustrated and analyzed later in Section IV.

Fig. 4 shows the calculation and the simulation results of $G_{vc}(s)$ with duty cycles of 0.1, 0.5, and 0.9. The simulation results are obtained from SIMPLIS. As can be seen, the calculation results are well-matched with the simulation results, indicating the validity of the mathematical model represented by (1). In Fig. 4, the Q-value at the half-switching frequency increases with the increase of the duty cycle, which verifies that the Q-value varies as the duty ratio varies. Note that, Fig. 4 is calculated at a given condition that C_T is 700 pF, R_i is 0.05 V/V, G_m is 1.5 mA/V, L_s is 250 nH, and f_{sw} is 500 kHz.

With a similar methodology, the output impedance, $Z_o(s)$, can be derived and simplified as well, as shown in the following:

$$Z_o(s) \approx K_z \frac{s}{s/\omega_a + 1} \frac{1}{1 + \frac{s}{Q_1\omega_1} + \frac{s^2}{\omega_1^2}} \frac{1}{1 + \frac{s}{Q_2\omega_2} + \frac{s^2}{\omega_2^2}} \tag{3}$$

where

$$K_z = \frac{L_s C_T R_L}{g_m T_{\text{sw}} R_i (1 - R_L k_2)}.$$

Evidently, Q_2 at the half-switching frequency also appears in the output impedance, which implies the load transient performance will be affected by Q-value variation under a wide-duty-range operation.

Fig. 5 shows the calculation and the simulation results of $Z_o(s)$ with duty cycles of 0.1, 0.5, and 0.9. As can be seen, the calculation results are again well-matched with simulation results, and Q-value clearly changes with the duty cycle.

To further explore the effect of Q-value on load transient performance, a step response simulation can be performed on the closed-loop output impedance. Here, the closed-loop output impedance, Z_{oc}, is defined as $Z_o(s)/[1 + T(s)]$, and $T(s)$ is the loop gain, which is defined as the sum of gain around the feedback loop (i.e., $T(s) = G_{vc}(s) \times H_v(s)$ in Fig. 2). For the closed-loop compensation, $H_v(s)$, a simple type II compensation with pole/zero cancellation is applied. The step-response results with Q-values of 0.6 and 4 are shown in Fig. 6. It can be seen that the ringing effect is exacerbated as the Q-value is increased. Therefore, a well-controlled Q-value is typically required to optimize the load transient behavior and prevent excessive undershoot/overshoot in a wide-duty-range operation. It is worth mentioning that this closed-loop transient analysis is not specifically applied to the UFTCOT control scheme; instead, the step response of closed-loop impedance analysis can be performed in any COT control scheme. In such a system with a high Q value, an excessive ringing phenomenon will occur [16].

As for the outer voltage regulation loop effect on the system stability and Q-value, unlike some of the literature [17], which views the whole system with the voltage regulation loop as a single entity in their models, which is also known as a closed-loop system, (1) and (3) are modeled by a DF [15], which views systems excluding outer voltage loop as a single entity, which is known as an open-loop system. In this way, the design of the control-to-output transfer function, $G_{vc}(s)$, and the outer

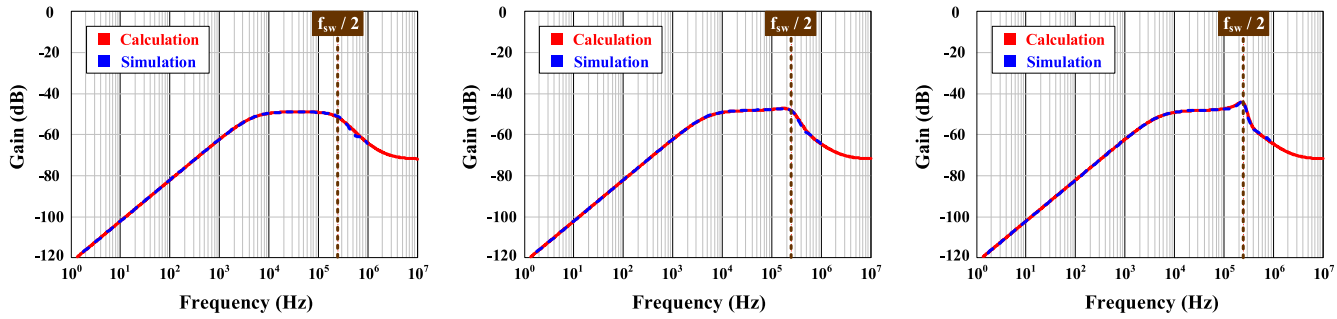

Fig. 5. Output impedance transfer function validation. (a) D = 0.1, Q-value = 0.64. (b) D = 0.5, Q-value = 0.96. (c) D = 0.9, Q-value = 2.39.

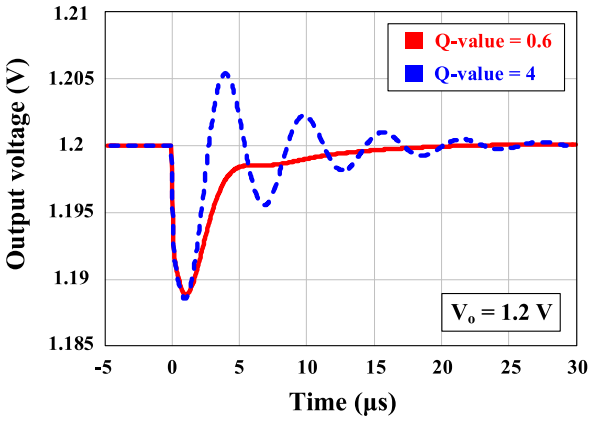

Fig. 6. Step response of the output impedance.

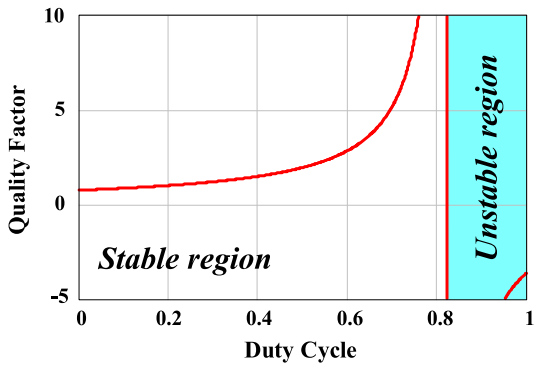

Fig. 7. Q-value variation without constant Q-value control.

voltage regulation loop, $H_v(s)$, can be effectively decoupled. That is, the stability of an open-loop system can be analyzed by RHP pole law, and the stability of a closed-loop system can be analyzed by loop gain, $T(s)$, with bode gain/phase margins criteria. Hence, the outer voltage regulation loop will be excluded in this article since the system is decoupled into $G_{vc}(s)$, and $H_{v(s)}$ design, In such case, $H_v(s)$ design generally focuses on a low-frequency domain, which is well below the half-switching frequency, and typically does not affect the Q-value at high-frequency domain.

III. Proposed Constant Q-Value Analysis for a Wide-Duty-Range Operation

From the preceding analysis, it is clear that Q_2 varies with the employed duty cycle, which can lead to stability issues in wide input-to-output voltage range applications. In this section, a generalized approach is presented, enabling a constant Q-value design that is independent of the duty cycle. Then, a constant Q circuit is proposed based on the UFTCOT control scheme.

A. Constant Q-Value Analysis

The stability criteria in (2) can be rearranged as follows to investigate the effect of duty cycle on Q-value:

$$\frac{C_T L_S}{R_i g_m T_{\text{sw}}} > \frac{D T_{\text{sw}}}{2}. \tag{4}$$

Here, the key variables at play are duty cycle and switching frequency since the other variables can be viewed as constants once the controller is designed. To reduce frequency variation caused by wide input/output voltage range in commercial products, an adaptive on-time (AOT) technique, which automatically adjusts the on-time according to input/output voltage, can be employed [18]. In this case, a fixed frequency can be presumed during steady-state operation. Consequently, the Q-value only varies with duty cycle. Fig. 7 shows this Q-variation versus duty cycle under baseline UFTCOT control scheme with AOT. Once the Q-value becomes negative, the system becomes unstable, as highlighted in the cyan-colored region. Note that Fig. 7 is calculated at a given condition that C_T is 700 pF, R_i is 0.05 V/V, G_m is 4 mA/V, L_s is 470 nH, and f_{sw} is 500 kHz.

As aforementioned, the key parameter at play in setting the Q-value is the duty cycle, which varies in wide input-to-output voltage applications. Hence, to achieve a constant Q-value, there should be another variable, that is capable of eliminating the effect caused by a wide input-to-output voltage range. To make the forthcoming discussion more clear, the variables that vary as the operation condition change are defined as control inputs (i.e., duty cycle, D, output voltage, V_o, and input voltage, V_{in}). Finally, a generalized analysis is developed, involving the following three steps.

1) Simplify the Q-value expression and identify which variable(s) can be deliberately designed to vary as control inputs changes.

2) Evaluate the relationship between the targeted variable(s) and the control inputs.
3) Design the targeted variable(s) to compensate for the effect caused by the control inputs.

Based on this, the following steps are performed to design a constant Q-value circuit for UFTCOT control. First, the expression for Q-value can be simplified to (5). Here, the variable that can be manipulated is the threshold voltage, V_{th}, since the other variables, including C_T, g_m, L_s, and R_i, are typically determined once the system is designed and they cannot be easily designed to vary as the operation point varies. Second, with V_{th} identified as a target variable, its relationship with the control inputs, namely duty cycle and V_o in this case, can be examined. The denominator of (5) is a function of V_o multiplied by the threshold voltage, which is then subtracted by a constant multiplied by the duty cycle. Therefore, V_{th} should also vary at the same rate as the duty cycle and V_o vary. Third, by observation, V_{th} should be a function of V_o to compensate for the Q-variation affected by V_o. However, if V_{th} is merely a function of V_o, the Q-value still varies with duty ratio. Hence, V_{th} should also be a function of duty cycle. Thus, V_{th} can be designed as $(\alpha + \beta D) \times V_o$. This gives a new Q-value, Q_2'', which can be expressed as (6), where α decides the exact Q-value, and β helps achieves a duty-independent Q-value

$$Q_2 = \frac{T_{\text{sw}}}{\pi} \frac{1}{\left(\frac{C_T L_s}{g_m R_i T_{\text{sw}}} \frac{V_{\text{th}}}{V_o} - \frac{T_{\text{sw}}}{2} D\right)} \tag{5}$$

$$Q_2'' = \frac{T_{\text{sw}}}{\pi} \frac{1}{(Q_{\text{init}} + a_1 D - a_2 D)} \tag{6}$$

where

$$Q_{\text{init}} = \frac{C_T}{g_m} \frac{L_s}{R_i} \frac{\alpha}{T_{\text{sw}}}, \quad a_1 = \frac{C_T}{g_m} \frac{L_s}{R_i} \frac{\beta}{T_{\text{sw}}}, \quad a_2 = \frac{T_{\text{sw}}}{2}$$

$$\alpha = \text{Const.}, \quad \beta = \frac{g_m R_i T_{\text{sw}}^2}{2 C_T L_S}. \tag{7}$$

There are several advantages to designing V_{th} as $(\alpha + \beta D) \times V_o$ as follows.

1) The output voltage is eliminated in (6), since the output voltage in V_{th} reduces the fraction in (5).
2) It is easy to achieve a constant Q-value. Once a_1 equals a_2, the effect of duty cycle is canceled out; namely, once (7) holds, the constant Q-value condition holds.
3) The Q-value can be simplified as (8) when (7) holds. That is, the exact value of the quality factor can be designed by the gain α when other parameters are determined. The lower the gain α is, the higher the Q-value will be.

In this way, the constant Q-value over the whole duty-cycle range can be achieved, and the exact value of Q is well-controlled

$$Q_2'' = \frac{T_{\text{sw}}^2 R_i g_m}{\pi C_T L_s} \frac{1}{\alpha}. \tag{8}$$

Fig. 8 shows a plot of Q-value versus duty cycle of the UFTCOT control with constant Q-value activated where the Q-value is designed to be 0.774 with $\alpha = 1$, and $\beta = 1.216$. It can be seen that with proper α and β design, a constant Q-value can be achieved.

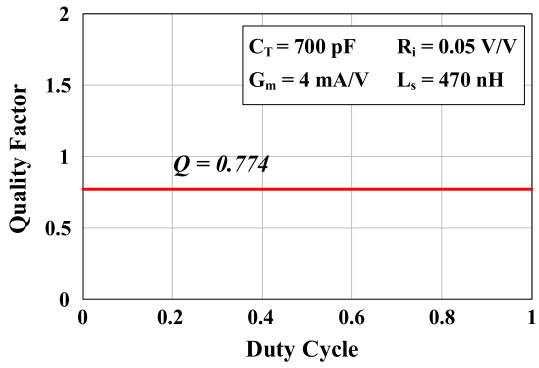

Fig. 8. Q-value variation with constant Q-value control.

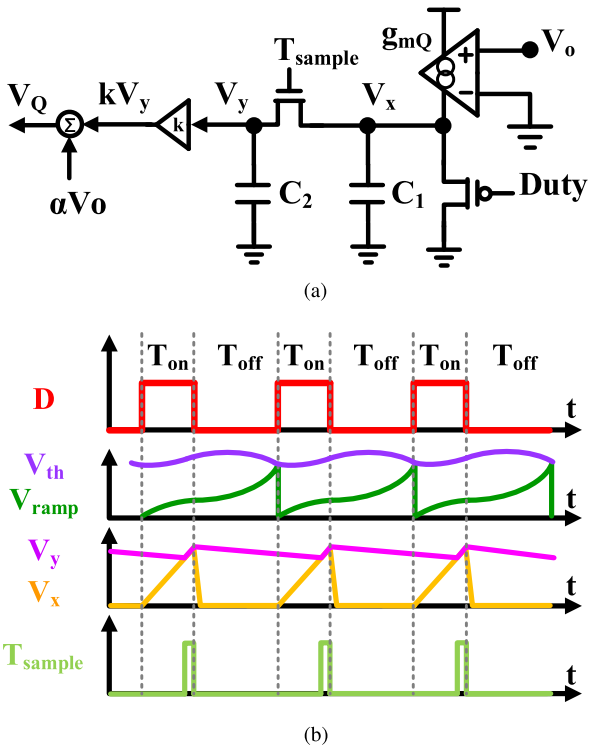

Fig. 9. $(\alpha + \beta D) \times V_o$ circuit and waveforms. (a) $(\alpha + \beta D) \times V_o$ generation circuit. (b) Key waveforms for $(\alpha + \beta D) \times V_o$ generation.

B. Constant-Q Circuit Design

One potential circuit to generate $(\alpha + \beta D) \times V_o$ and achieve the constant Q-value is shown in Fig. 9(a), with key waveforms shown in Fig. 9(b). When the duty signal is high, the capacitor, C_1, is charged by a current generated from the output-voltage-controlled transconductor, generating voltage, V_x, which is then sampled by the sampling signal, T_{sample}, and stores the value to the capacitor, C_2. The sampled voltage, V_y, is connected to a gain stage with a gain of k, and then adds to αV_o to create a constant Q-value control voltage V_Q. When the duty signal is low, the switch in parallel with C_1 is activated and purges the charge stored in C_1, resetting and clamping V_x to zero. At the same time, C_2 holds the sampled voltage, V_y.

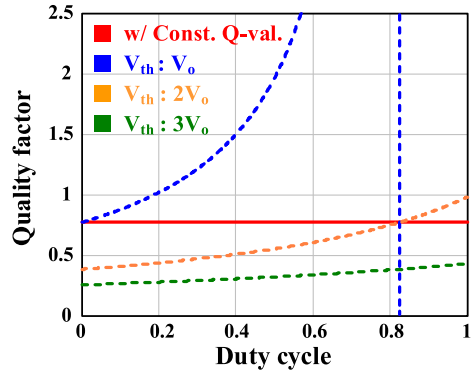

Fig. 10. Q-value variation of UFTCOT control scheme.

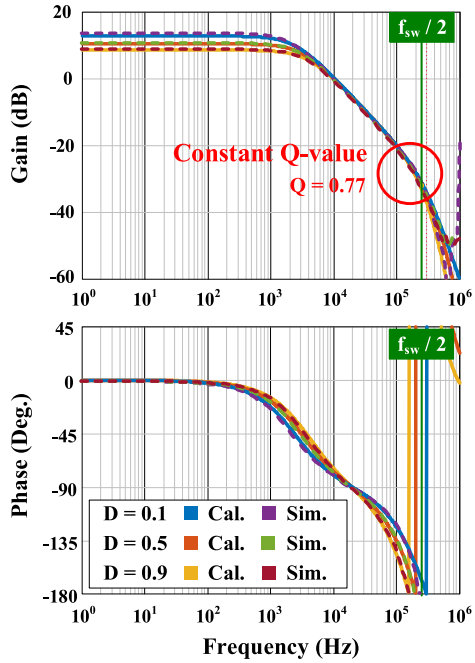

Fig. 11. Control-to-output transfer function of UFTCOT control scheme.

Eventually, the final output, V_Q, of the proposed circuit is found as $(\alpha V_o + kV_y)$. To ensure $V_{\text{th}} = (\alpha + \beta D) \times V_o$, kV_y should be equal to $\beta D V_o$, where kV_y can be found as (9) by the charging equation $(Q = C \times V = I \times T)$, and $\beta D V_o$ can be written as (10). Then, $(k \times g_{mQ})/C_1$ can be designed to be equal to $\beta \times f_{\text{sw}}$ to make V_Q equal $(\alpha + \beta D) \times V_o$, achieving a constant Q-value. Note that β is shown in (7).

$$kV_y \approx k\frac{g_{mQ}}{C_1} T_{\text{on}} V_o \tag{9}$$

$$\beta D V_o = \beta f_{\text{sw}} T_{\text{on}} V_o. \tag{10}$$

Fig. 10 shows the Q-value variations with different threshold voltages along with the Q-value with constant Q-value circuit enabled. Fig. 11 shows $G_{vc}(s)$ of UFTCOT with the constant Q-value circuit enabled under different duty-cycle conditions in both calculation and simulation where Q-value is designed to be approximately 0.77, where the parameters used are the same as in Fig. 8. It can be seen that the Q-value at the half-switching frequency is well-controlled and duty-cycle-independent under different duty-ratio conditions. It should be noted that the phase difference at high frequencies (i.e., around the half-switching frequency) is caused by the high-frequency complex poles at ω_1, as shown in (1).

One of the caveats while adopting the constant Q-value control is that although the constant Q-value control minimizes the Q-variation at the half-switching frequency over wide input/output operations, the dc gain and low-frequency pole(s) in the small-signal models can be slightly different after applying the constant Q-value control, where the difference is subject to change with different control schemes and constant Q-value strategies employed. Here, based on (1) with constant Q-vlaue control presented in Fig. 9, the dc gain and dominant pole of UFTCOT control scheme will typically be slightly lower and higher, respectively. Luckily, the $G_{vc}(s)$ difference can be easily compensated by the outer voltage regulation loop design. That is, with a proper $H_V(s)$, as shown in Fig. 2, design, the total loop gain, $T(s)$, can be the same as the loop gain without the constant Q-value control; hence, the transient performance is not be sacrificed due to the constant Q-value control.

C. Effects of System Component and Constant Q-Value Voltage Tolerance on Constant Q-Value Accuracy

In the actual circuit implementation, the component tolerance and accuracy of the constant Q-value circuit often come into play and degrade the effectiveness of the constant Q-value control, even when the constant Q-value is carefully designed. In this section, the effect of the component and constant Q-value control voltage, V_Q, tolerance is illustrated and summarized.

1) Effect of Component Tolerance on Q-Variation: Here, two assumptions have been made for this analysis: 1) a perfect Q-value circuit is assumed, and the component tolerance occurs only on the power stage and modulator components, e.g., R_i, L_s, G_m, etc; 2) $\pm 5\%$ variance in a Gaussian distribution is assumed for each component. With these two assumptions, a 50 000-point Monte Carlo simulation is performed. Note that the parameters for the calculation are the same, as used in Fig. 8. The resulting Q-value variation distribution is shown in Fig. 12(a). Here, Q-value variations at D = 0, 0.5, and 1 cases are plotted. It can be observed that with a larger duty cycle, a higher Q-variation is shown where the standard deviation increases from 0.018 to 0.04 as the duty cycle moves from 0 to 1. This also implies that Q-value varies to a higher/lower value at a larger duty cycle that Q_{max} moves from 0.85 to 0.97, and Q_{min} moves from 0.79 to 0.62 as D moves toward 1 from 0. The Q-value variation with duty cycle is shown in Fig. 12(b). Here, the orange shaded area shows the potential Q-value curves where the area with a higher intensity implies a higher possibility of Q-vlaue curve to be. It can be found that the Q-value shows a maximum and minimum of 26% and –19% deviation, respectively, toward the targeted constant Q-value when component tolerance is in play. In addition, the Q-value variation with the duty cycle is no longer constant but a value between -11% and 14% variation due to the component tolerance. Nevertheless, compared to the original

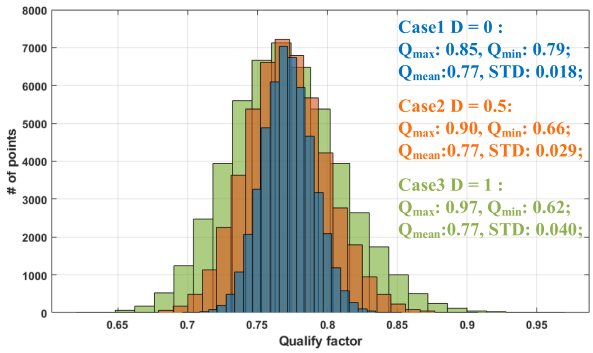

(a)

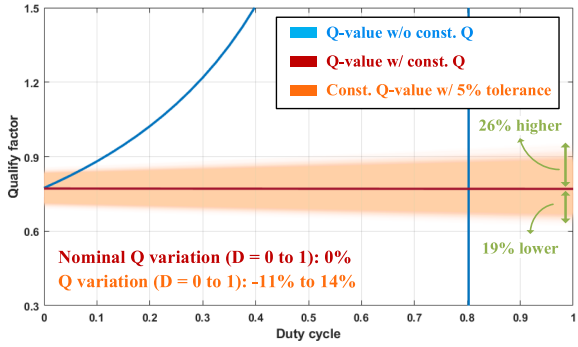

(b)

Fig. 12. Component tolerance effect on Q-value variation. (a) Q-value Monte Carlo simulation with 5% component tolerance. (b) Q-value variation versus duty cycle.

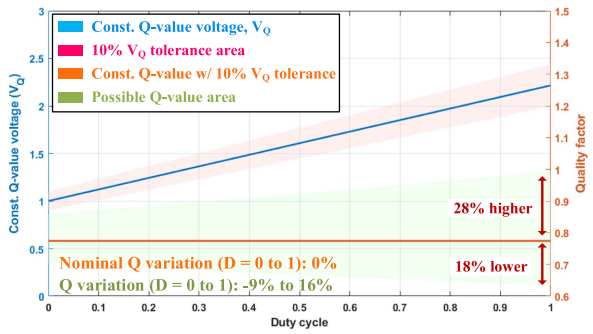

Fig. 13. Q-value variation with $\pm 10\%$ V_Q tolerance.

Q-variation curve without constant Q-value control, the Q-value control strategy significantly improves the system stability no matter whether there is component tolerance or not.

2) Effect of V_Q Tolerance on Q-Variation: Aside from the component tolerance, the constant Q-value control voltage, V_Q, generated from the constant Q-value circuit can sometimes deviate from the design value. Here, $\pm 10\%$ V_Q tolerance and tolerance-free components are assumed. The Q-value variation with duty is shown in Fig. 13. The V_Q tolerance shows similar trends with component tolerance, where the maximum and minimum Q-value variations are –18% and +28% compared to the design value at $+10\%$ and -10% V_Q tolerance cases, respectively, and the percentages of variations due to the duty

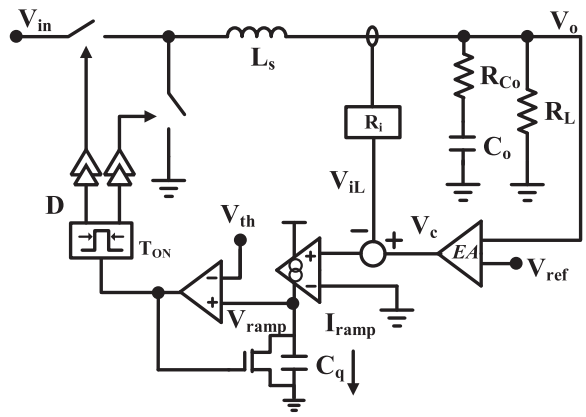

Fig. 14. IQCOT control circuit diagram.

cycle are from -9% to $+16\%$ under $\pm 10\%$ V_Q cases. Again, even with V_Q tolerance, the constant Q-value control can stabilize the system and enable the system to be operated at a higher duty cycle range.

IV. Extending to Other Existing Control Schemes

The constant Q-value analysis can be easily extended to a variety of COT controllers since the proposed constant Q-value method does not alter the original modulation law of a COT control scheme and, therefore, the COT models reported can be directly reused and analyzed. Three state-of-the-art COT control schemes and a general form of an RBCOT with continuous ramp compensation are presented and analyzed to achieve constant Q-value in this section:

1) inverse charge COT (IQCOT) control [5];
2) accurate adaptive COT (A^2COT) control [8];
3) RBCOT with virtual inductor current (RBCOT with VIC) control [9];
4) RBCOT control with continuous ramp compensation.

A. IQCOT Control Scheme

The circuit diagram of IQCOT control scheme [5] is shown in Fig. 14, which is very similar to UFTCOT control, but instead with inductor current sensing and a constant threshold voltage. Therefore, the small-signal models of IQCOT control, shown in [5], is similar to UFTCOT control.

The Q-value expression at $f_{sw}/2$ is described as (5), which is the same as UFTCOT, shown in (1). Therefore, the same method can be applied to the IQCOT control, which designates the threshold voltage to be $(\alpha + \beta D) \times V_o$. Moreover, the constant Q-value circuit proposed in Section III can be applied as well. As a result, a constant Q-value can be realized, and the new Q-value expression is shown in (6), which is the same as UFTCOT control. The constant Q-value validation can refer to Fig. 11 since its $G_{vc}(s)$ is similar to UFTCOT control [5], [12].

B. A^2COT Control Scheme

For the A^2COT control scheme [8], the Q-value expression at $f_{sw}/2$ is described by (11). Given this expression, the constant

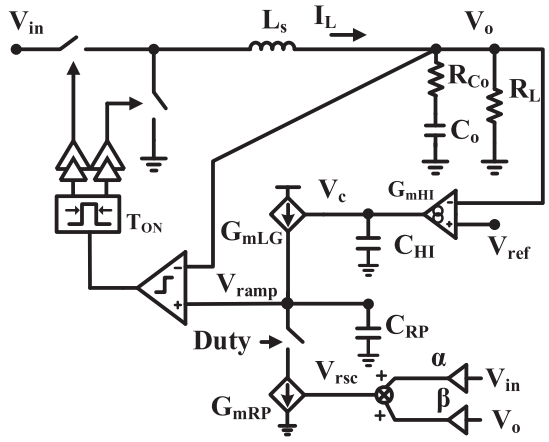

Fig. 15. A^2COT control circuit diagram with constant Q-value circuit.

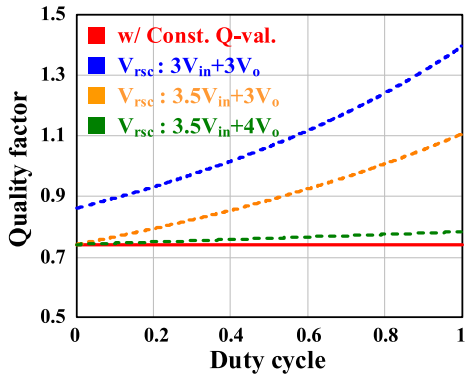

Fig. 16. Q-value variation of A^2COT control scheme.

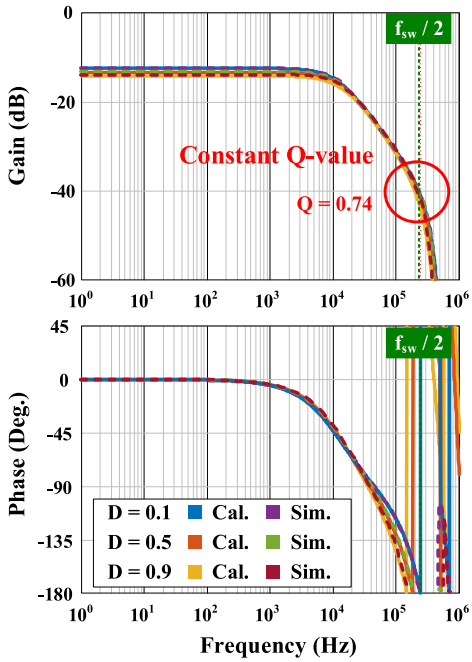

Fig. 17. Control-to-output transfer function of A^2COT control scheme.

Q-value concept can be applied as follows. 1) The variable that can be adjusted is the ramp-slope-control voltage, $V_{\rm rsc}$ in the Q-value expression, since other variables are usually determined once system is designed. 2) The relationship between $V_{\rm rsc}$ and the control inputs, duty ratio, and input voltage in this case, can be identified. 3) By observation, $V_{\rm rsc}$ should eliminate the Q-value variation caused by the input voltage and the duty cycle at the same time. Interestingly, if $V_{\rm rsc}$ is a function of the input voltage and output voltage such as $(\alpha V_{\rm in} + \beta V_o)$, then the $\alpha V_{\rm in}$ term can be used to eliminate $V_{\rm in}$ variation in (11), while the βV_o term forms a duty cycle term because of $(D = V_o/V_{\rm in})$ and can be used to cancel out the $T_{\rm sw}/2 \times D$ term in (11).

Combining the previous observations, $V_{\rm rsc}$ can be designated to be $(\alpha V_{\rm in} + \beta V_o)$ and the constant Q-value expression can be derived as (12), where α decides the exact Q-value, and β achieves constant Q-value. Again, the input voltage is eliminated in the new expression. Also, if a_1 is equal to a_2, the effect of duty-cycle variation can be eliminated. Subsequently, the exact value of the quality factor can be designed via α in $Q_{\rm init}$.

Importantly, the input/output controlled $V_{\rm rsc}$ is naturally built-in; namely, there is no additional circuit required in A^2COT to achieve a constant Q-value, as shown in Fig. 15.

Fig. 16 shows the Q-value variations with different ramp-slope-control voltages, $V_{\rm rsc}$, along with the Q-value with constant Q-value circuit enabled. In [8], a nearly constant Q-value is claimed, as shown in Fig. 16, when $V_{\rm rsc}$ is $3.5V_{\rm in} + 4V_o$; however, the constant Q-value could, in fact, be achieved by the systematic analysis proposed in (12). Fig. 17 shows $G_{vc}(s)$ of A^2COT with the constant Q-value circuit enabled under duty cycles of 0.1, 0.5, and 0.9, where the validity of $G_{vc}(s)$ is proven in [8]. It can be seen that the Q-value at the half-switching frequency is well-controlled and duty-cycle-independent, where no peaking is shown in the magnitude plot at the half-switching frequency as the duty cycle increases

$$Q_2 = \frac{T_{\rm sw}}{\pi\left[\left(R_{C_o}C_o + \frac{L_s G_{mRP} R_{C_o} C_o}{C_{RP} R_i}\frac{V_{\rm rsc}}{V_{\rm in}}\right) - \frac{T_{\rm sw}}{2}D\right]} \tag{11}$$

$$Q_2'' = \frac{T_{\rm sw}}{\pi}\frac{1}{(Q_{\rm init} + a_1 D - a_2 D)} \tag{12}$$

where

$$Q_{\rm init} = R_{C_o}C_o + \frac{L_s G_{mRP} C_o}{C_{RP}}\alpha$$

$$a_1 = \frac{L_s G_{mRP} C_o}{C_{RP}}\beta, \quad a_2 = \frac{T_{\rm sw}}{2}.$$

C. RBCOT With VIC Control Scheme

The Q-value of the RBCOT with VIC control scheme [4] is shown in (13). As in the previous sections, the constant Q-value concept can be employed as follows.

1) The ramp slope, M_f, is substituted into (13), but, after simplification, there is no variable that can be controlled. Hence, going back to the original expression (13), it can

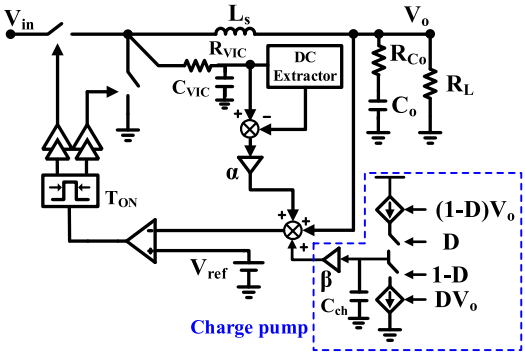

Fig. 18. RBCOT w/ VIC control circuit diagram with constant Q-value circuit.

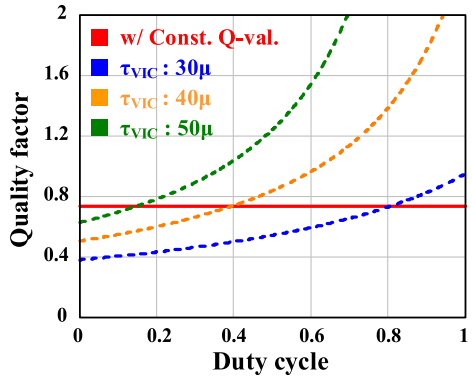

Fig. 19. Q-value variation of RBCOT w/ VIC control scheme.

be seen that the ramp slope, M_f, is the variable that can be modulated.

2) The relationship between M_f and the control inputs, which are duty cycle and V_o in this case, can be identified. M_f should be capable of eliminating the Q variations caused by duty cycle and V_o variation.
3) Then, M_f needs to be redesigned, and according to step 1, the original M_f is capable of eliminating V_o variation but unable to compensate the duty-cycle variation. As a result, a duty-cycle compensation term should be added in to the original M_f. Finally, the new M_f can be designated as (14)

$$Q_2 = \frac{T_{\rm sw}}{\pi\left[\left(1+\frac{L_s M_f}{R_i V_o}\right) R_{C_o} C_o - \frac{T_{\rm sw}}{2} D\right]} \tag{13}$$

where

$$M_f = \frac{\alpha V_o}{R_{\rm VIC} C_{\rm VIC}}$$

$$M_f'' = \frac{\alpha V_o}{R_{\rm VIC} C_{\rm VIC}} + \frac{\beta D V_o}{R_{\rm VIC} C_{\rm VIC}}. \tag{14}$$

After designating M_f'', the Q-value can be rearranged as (15), where, again, α decides the exact Q-value, and β achieves constant Q-value. Similar to other constant Q-value expressions, when a_1 is equal to a_2, the effect of duty-cycle variation can be eliminated. Thereafter, the exact value of the quality factor can be designed via α in $Q_{\rm init}$. In this way, the instability issue can be effectively addressed

$$Q_2'' = \frac{T_{\rm sw}}{\pi} \frac{1}{(Q_{\rm init} + a_1 D - a_2 D)} \tag{15}$$

where

$$Q_{\rm init} = R_{C_o} C_o + \frac{L_s C_o}{R_{\rm VIC} C_{\rm VIC}} \alpha$$

$$a_1 = \frac{L_s C_o}{R_{\rm VIC} C_{\rm VIC}} \beta, \quad a_2 = \frac{T_{\rm sw}}{2}.$$

To achieve a constant Q-value in RBCOT with VIC control, an additional ramp generation is required to generate the second term in (14). A simple charge pump circuit can be applied to the generate ramp compensation, as shown in Fig. 18. The charge pump circuit consists of two output-voltage-controlled current sources, which are controlled by switches that are controlled by the input duty signal and its complement, to charge and discharge a capacitor generating the ramp and then, connect to a gain stage with a gain of β. The charge and discharge time is determined by D and $1-D$. Note that the charge pump circuit is a simplified version for functional illustration purposes only.

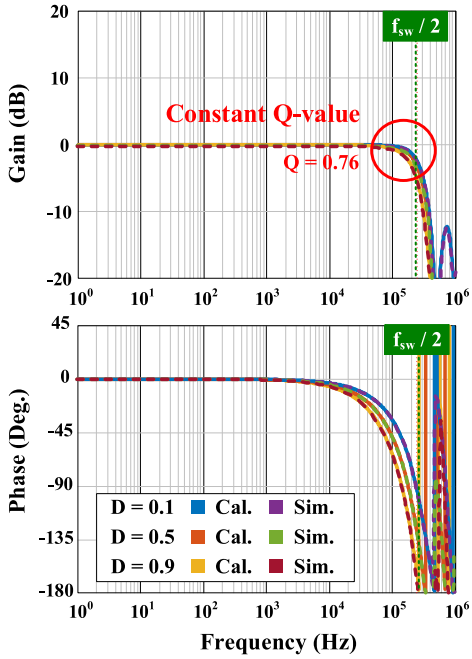

Fig. 20. Control-to-output transfer function of RBCOT w/ VIC control scheme.

Fig. 19 shows the Q-value variations with different VIC time constant, $\tau_{\rm VIC} = R_{\rm VIC} C_{\rm VIC}$, along with the Q-value with constant Q-value circuit enabled. It can be found that when the constant Q-value circuit is not enabled, quality factors vary with the duty cycle, and the variation depends on $\tau_{\rm VIC}$ applied, which causes design difficulties as discussed in Figs. 1 and 6. On the other hand, the Q-value can be well-controlled with the design rule proposed in (15). Fig. 20 shows the calculated and simulated $G_{vc}(s)$ of RBCOT w/ VIC with the constant Q-value circuit enabled under different duty-cycle conditions,

where the validity of $G_{vc}(s)$ is proven in [4]. It can be seen that the Q-value at the half-switching frequency is well-controlled and duty-cycle-independent, that no peaking is presented with duty-cycle varying.

D. RBCOT Control With Continuous Ramp Compensation

In addition to the ripple-based control schemes mentioned in Section IV(b) and (c), the proposed constant Q-value control concept can also be applied to most other RBCOT-controlled buck converters with continuous ramp compensation, where the continuous ramp refers to the type of ramp compensation without resetting the ramp to zero in a cycle [4], [8], [9], [13], [14], [19], [20]. Note that RBCOT with discontinuous ramp compensation control schemes, [2], [10], [11], [21], [22], [23], are out of scope in this article.

In general, the Q-value of RBCOT with continuous ramp compensation control schemes can be simplified as (16) where S_{ramp} stands for the ramp compensation slope added to the RBCOR control that enhances to equivalent ESR, and S_f is sensed inductor current slope due to output voltage ripple in RBCOT modulation. It is worth mentioning that S_{ramp} is subject to change in different control schemes and implementations, and to make an in-phase ramp with the inductor current that enhances equivalent ESR, S_{ramp} is typically a function of V_o, i.e., (13). Hence, S_{ramp} is assumed to be a function of V_o with a constant gain, K_{ramp}, here

$$Q_2 = \frac{T_{\text{sw}}}{\pi\left[\left(1+\frac{S_{\text{ramp}}}{s_f}\right)R_{C_o}C_o - \frac{T_{\text{sw}}}{2}D\right]} \tag{16}$$

where

$$s_f = R_{Co}\frac{V_o}{L_s}, \quad S_{\text{ramp(typ.)}} = K_{\text{ramp}}V_o.$$

With (16), the constant Q-value strategy can be applied as follow.

1) Simplify the Q-value expression, as shown in (17), by substituting S_f into (16).
2) The relationship between S_{ramp} and the control inputs, which are duty cycle and V_o in this case, can be identified. S_{ramp} should be capable of eliminating the Q variations caused by duty cycle and V_o variation.
3) S_{ramp}, then, needs to be redesigned, and according to step 1, the original S_{ramp} is capable of eliminating V_o variation but unable to compensate the duty-cycle variation. As a result, a duty-cycle compensation term should be added to the original S_{ramp}.

Finally, the new ramp slope can be designated as (18), and the Q-value expression can be rewritten as (19). A constant Q-value can be achieved while a_1 equals a_2 and the Q-value can be set by Q_{init}.

$$Q_2 = \frac{T_{\text{sw}}}{\pi\left[\left(1+\frac{L_s S_{\text{ramp}}}{R_{C_o}V_o}\right)R_{C_o}C_o - \frac{T_{\text{sw}}}{2}D\right]} \tag{17}$$

$$S''_{\text{ramp}} = K_{\text{ramp}}\left(\alpha+\beta D\right)V_o \tag{18}$$

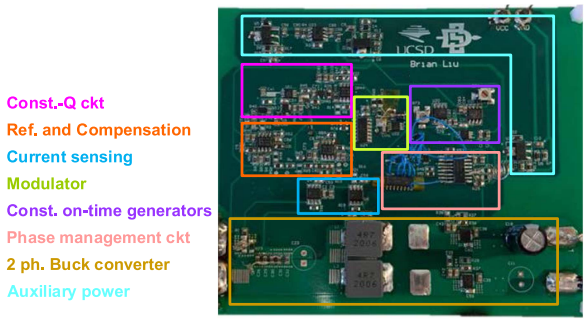

Fig. 21. PCB design for UFTCOT control scheme with Constant Q-value control.

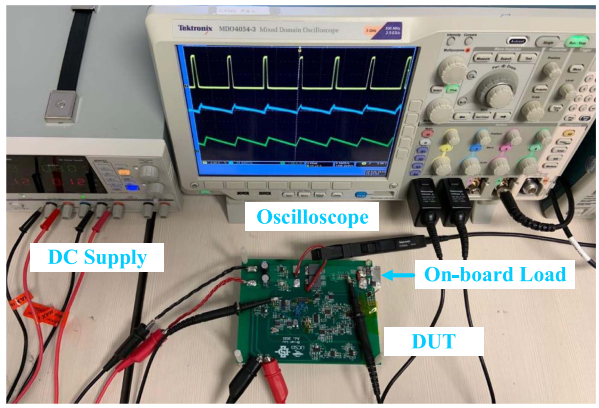

Fig. 22. Experiment setup of the UFTCOT control scheme.

$$Q''_2 = \frac{T_{\text{sw}}}{\pi}\frac{1}{(Q_{\text{init}}+a_1 D - a_2 D)} \tag{19}$$

where

$$Q_{\text{init}} = R_{Co}C_o + C_o L_s K_{\text{ramp}}\alpha$$

$$a_1 = C_o L_s K_{\text{ramp}}\beta, \quad a_2 = \frac{T_{\text{sw}}}{2}.$$

V. Experimental Verification

A fully discrete buck converter with UFTCOT control is implemented to verify the proposed constant Q concept, as shown in Figs. 21 and 22, where the experimental parameters are listed in Table II. Note that: 1) Fig. 21 shares the same design as [12] and only one phase buck converter is enabled for the constant Q-value control verification in this article, 2) the capacitor current sensing of this prototype is implemented by the resistor sensing, where a small resistor is inserted, and the capacitor current is then measured by the resistor voltage. According to the parameters listed in Table II and (6), the quality factor of the system is approximately equal to 0.6 when the constant Q-value circuit is enabled.

Fig. 23 shows the modulation waveforms of the UFTCOT control scheme at 12/1 V, which works well and are similar to modulation law illustrated in Fig. 3. When the ramp voltage, V_{ramp}, is equal to the threshold voltage, V_{th}, the duty signal is triggered and V_{ramp} is reset to zero. Fig. 24 shows the steady-state

TABLE II
EXPERIMENTAL PARAMETERS

Parameters	Values
Input voltage range V_{in}	1.5-12 V
Output voltage range V_o	1.2 V
Output current range I_o	0 - 10 A
Switching frequency f_{sw}	$\approx$ 300 kHz
Output inductor L_s	4.7 μH
Output capacitor C_o	220 μF
Equivalent series resistance ESR	10 mΩ
Threshold capacitor C_T	1 nF
Modulator transconductance g_m	8 mA/V
Sensing gain R_i	0.1 V/A
Const. Q-value ckt. Transconductance g_{mQ}	1 mA/V
Const. Q-value ckt. capacitor 1 C_1	1 nF
Const. Q-value ckt. capacitor 2 C_2	100 pF
Const. Q-value ckt. V_y gain k	2.8 V/V
Const. Q-value ckt. V_o gain α	1 V/V

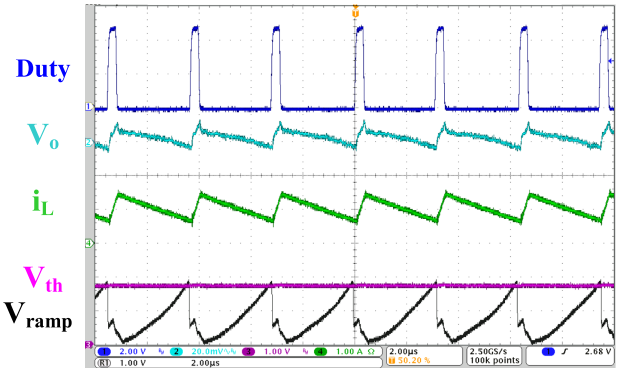

Fig. 23. Modulation waveforms at D $\approx$ 0.1, 12–1.2 V, Q $\approx$ 0.6.

waveforms at different duty cycles to verify the modulation and proposed constant Q-value circuit. It can be seen that the threshold voltage, V_{th}, is well-matched with the $(\alpha + \beta D) \times V_o$ concept that, with a higher duty cycle, a higher V_{th} is generated to control the Q-value of the system. Fig. 25 shows the steady-state waveforms when the duty cycle is equal to 50% with and without constant Q-value circuit. With the constant Q-value circuit, the system can operate stably, as shown in Fig. 25(a). In contrast, the system shows subharmonic oscillations without the constant Q-value circuit, as shown in Fig. 25(b), implying system instability. Note that, to simulate the unstable condition, the circuit parameters are deliberately adjusted, which are thus not exactly the same, as in Table II. Still, both stable and unstable conditions in Fig. 25 are tested under the same parameter setup.

The accuracy of the proposed constant Q-value circuit is essential in guaranteeing constant Q-value during operation since there are many error sources involved in V_Q generation, such as mismatch, noise, and so on. To determine how many errors are generated during sample and hold, amplifying, and summing, the accuracy of the constant Q-value is measured. In Fig. 26, the left y-axis shows the voltage and Q-value, while the

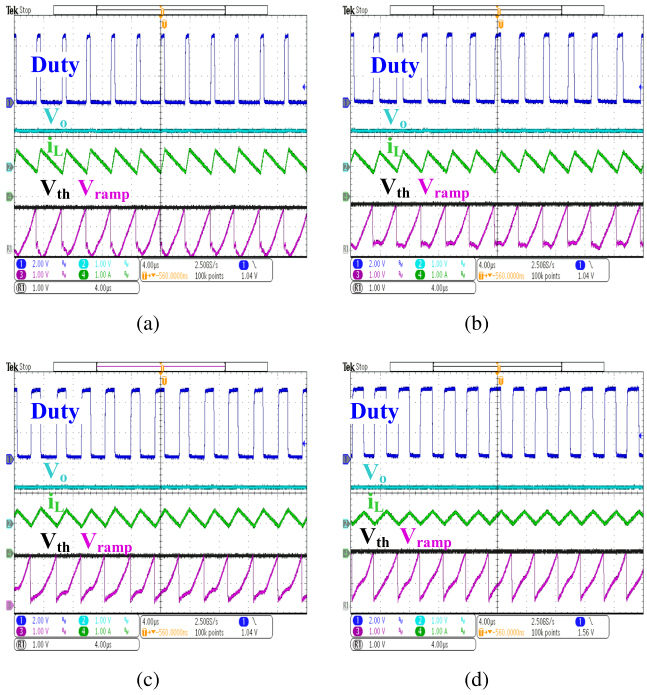

Fig. 24. Steady-state operation waveforms at different duty cycle, Q $\approx$ 0.6. (a) D $\approx$ 0.15, 8–1.2V. (b) D $\approx$ 0.25, 5–1.2V. (c) D $\approx$ 0.38, 3.3–1.2V. (d) D $\approx$ 0.5, 2.5–1.2V.

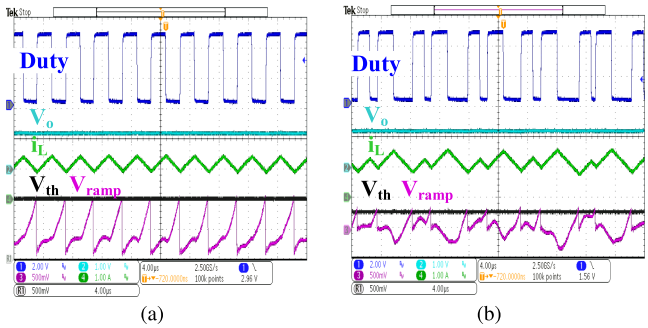

Fig. 25. Operation waveforms at $\approx$ 50% duty cycle, 2.5–1.2 V. (a) Stable operation, $\alpha = 0.3$, $\beta = 0.93$, (constant Q-value circuit enabled). (b) Unstable operation, $\alpha = 0.3$, $\beta = 0$, (constant Q-value circuit disabled).

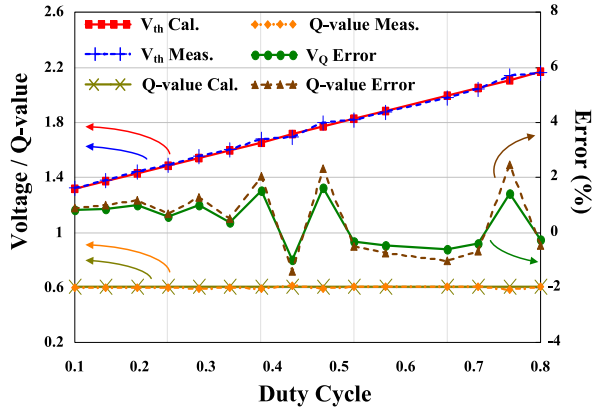

Fig. 26. Accuracy of constant Q-value circuit.

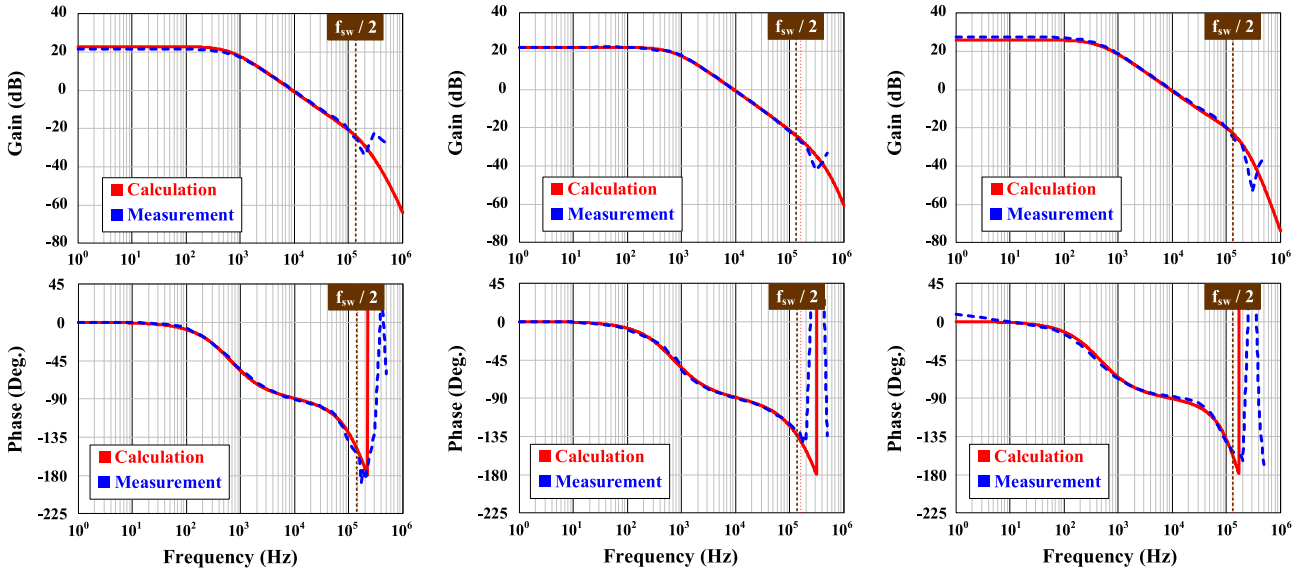

Fig. 27. Control-to-output transfer function measurement results for the UFTCOT control scheme with constant Q-value circuit enabled. (a) D ≈ 0.1, 12–1.2 V, Q ≈ 0.6. (b) D ≈ 0.25, 5–1.2 V, Q ≈ 0.6. (c) D ≈ 0.38, 3.3–1.2 V, Q ≈ 0.6.

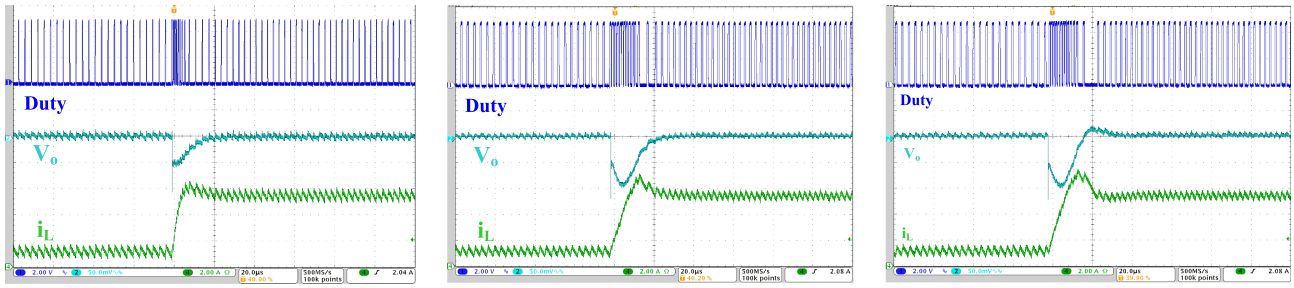

Fig. 28. Load transient response comparison with and without constant Q-value mechanism. (a) 12–1.2 V with constant Q-value ($Q \approx 0.6$). (b) 5–1.2 V with constant Q-value ($Q \approx 0.6$). (c) 5–1.2 V without constant Q-value ($Q \approx 0.8$).

right y-axis shows the percentage of the error. The calculation and measurement results of V_Q and Q-value, labeled at the top-left corner in Fig. 26, are shown in solid and dashed lines, respectively, referring to the left axis. On the other hand, the error of V_Q (V_Q error) and Q-value (Q-value error), labeled at the top-right corner in Fig. 26, are shown in solid and dashed lines referring to the right axis. Here, the error of the constant Q-value voltage (V_Q error) is less than 2%, and the error of the Q-value (Q-value error) is less than 3%. Note that, since the Q-value cannot be directly measured, the measured Q-value shown in Fig. 26 is obtained from (5) using actual circuit parameters, and measured V_Q, as shown in Table II and Fig. 26.

To verify the proposed constant Q-value method and circuit that is applied to the UFTCOT control scheme, the control-to-output transfer function of UFTCOT with the constant Q-value circuit is both calculated and measured, as shown in Fig. 27, where the transfer functions of 12, 5, and 3.3–1.2 V cases are conducted. It can be seen that the measurement results are matched with the calculation results implying that the Q-value is well controlled. Another worth mentioning point from the transfer function measurement results is that since the constant Q-value method proposed does not change the original modulation law of UFTCOT, the model reported in [12] can be directly applied, and the same logistics can also be applied to the rest of COT control schemes.

The constant Q-value circuit not only prevents the system instability in a wide-duty-range operation but also improves the load transient response. As discussed in Section II, the high Q-value in the output impedance will cause a ringing effect during a fast load transient. To test the fast load transient, an onboard load circuit is implemented with a slew rate of 50 A/μs. Fig. 28 shows the load transient response for different input voltage (12 and 5 V) while converting down to 1.2 V with and without the constant Q-value circuit. Fig. 28(a) shows the load transient response with a 12 V input voltage, which serves as a control. Fig. 28(b) and (c) shows the load transient response with

a 5 V input voltage with and without the constant Q-value circuit. It can be seen that the output voltage waveform in Fig. 28(a) and (b) does not exhibit ringing during the transient response. In contrast, from (1), the lower the input voltage is, the higher the Q-value will be, and therefore, Fig. 28(c) shows a ring back phenomenon because of a higher Q-value.

VI. Conclusion

This article has presented a generalized strategy to design a well-controlled and duty-cycle-independent quality factor for COT-controlled buck converters. A design example under a baseline UFTCOT control scheme is illustrated and verified by both simulations, calculations, and experiments. The constant Q-value circuit is capable of ensuring system stability and improving load transient response, all while alleviating high bandwidth design efforts in a COT buck controller over a wide input–output voltage range. The proposed design strategy is also extended and applied to several other state-of-the-art COT control schemes, as verified by both calculations and simulations. In summary, using the strategy presented in this article, a simple, well-controlled, and duty-cycle-independent Q-value can be achieved in most COT-controlled buck converters.

References

[1] J. Li and F. C. Lee, "Modeling of v^2 current-mode control," *IEEE Trans. Circuits Syst. I: Regular Papers*, vol. 57, no. 9, pp. 2552–2563, Sep. 2010.

[2] S. Tian, F. C. Lee, P. Mattavelli, K. Cheng, and Y. Yan, "Small-signal analysis and optimal design of external ramp for constant on-time v^2 control with multilayer ceramic caps," *IEEE Trans. Power Electron.*, vol. 29, no. 8, pp. 4450–4460, Aug. 2014.

[3] Texas Instruments, "D-cap mode with all-ceramic output capacitor application," 2011. [Online]. Available: https://www.ti.com/lit/an/slva453/slva453.pdf

[4] C. Chen, D. Chen, C. Tseng, C. Tseng, Y. Chang, and K. Wang, "A novel ripple-based constant on-time control with virtual inductor current ripple for buck converter with ceramic output capacitors," in *Proc. 26th Annu. IEEE Appl. Power Electron. Conf. Expo.*, 2011, pp. 1488–1493.

[5] S. Bari, Q. Li, and F. C. Lee, "High frequency small signal model for inverse charge constant on-time (IQCOT) control," in *Proc. IEEE Energy Convers. Congr. Expo.*, 2018, pp. 6000–6007.

[6] K. B. Cheng, F. C. Lee, and P. Mattavelli, "Adaptive ripple-based constant on-time control with internal ramp compensations for buck converters," in *Proc. IEEE Appl. Power Electron. Conf. Expo.*, 2014, pp. 440–446.

[7] T. Qian and B. Lehman, "An adaptive ramp compensation scheme to improve stability for dc–dc converters with ripple-based constant on-time control," in *Proc. IEEE Energy Convers. Congr. Expo.*, 2014, pp. 3424–3428.

[8] W. Liu, C. Chen, C. Cheng, and H. Chen, "A novel accurate adaptive constant on-time buck converter for a wide-range operation," *IEEE Trans. Power Electron.*, vol. 35, no. 4, pp. 3729–3739, Apr. 2020.

[9] Y. Lin, C. Chen, D. Chen, and B. Wang, "A ripple-based constant on-time control with virtual inductor current and offset cancellation for dc power converters," *IEEE Trans. Power Electron.*, vol. 27, no. 10, pp. 4301–4310, Oct. 2012.

[10] L. Kong, D. Chen, S. Hsiao, C. Nien, C. Chen, and K. Li, "A novel adaptive-ramp ripple-based constant on-time buck converter for stability and transient optimization in wide operation range," *IEEE Trans. Emerg. Sel. Topics Power Electron.*, vol. 6, no. 3, pp. 1314–1324, Sep. 2018.

[11] J. Li and F. C. Lee, "Modeling of V2 current-mode control," in *Proc. 24th Annu. IEEE Appl. Power Electron. Conf. Expo.*, 2009, pp. 298–304.

[12] W.-C. Liu, C.-H. Cheng, C. C. Mi, and P. P. Mercier, "A novel ultrafast transient constant on-time buck converter for multiphase operation," *IEEE Trans. Power Electron.*, vol. 36, no. 11, pp. 13096–13106, Nov. 2021.

[13] Y. Yan, P. Liu, F. Lee, Q. Li, and S. Tian, "V^2 control with capacitor current ramp compensation using lossless capacitor current sensing," in *Proc. IEEE Energy Convers. Congr. Expo.*, 2013, pp. 117–124.

[14] S. Tian, F. C. Lee, Q. Li, and Y. Yan, "Unified equivalent circuit model and optimal design of v^2 controlled buck converters," *IEEE Trans. Power Electron.*, vol. 31, no. 2, pp. 1734–1744, Feb. 2016.

[15] J. Li and F. C. Lee, "New modeling approach and equivalent circuit representation for current-mode control," *IEEE Trans. Power Electron.*, vol. 25, no. 5, pp. 1218–1230, May 2010.

[16] R. W. Erickson and D. Maksimovic, *Fundamentals of Power Electronics*, 3rd ed. Berlin, Germany:Springer, 2013.

[17] X. Zhang, Z. Zhang, H. Bao, B. Bao, and X. Qu, "Stability effect of control weight on multiloop COT-controlled buck converter with PI compensator and small output capacitor ESR," *IEEE Trans. Emerg. Sel. Topics Power Electron.*, vol. 9, no. 4, pp. 4658–4667, Aug. 2021.

[18] RichTek, "ACOT (advanced constant-on time) synchronous step-down converters" 2015. [Online]. Available: https://www.richtek.com/m/~/media/AN%20PDF/SG002_EN.pdf

[19] Y. Yan, F. C. Lee, S. Tian, and P.-H. Liu, "Modeling and design optimization of capacitor current ramp compensated constant on-time v^2 control," *IEEE Trans. Power Electron.*, vol. 33, no. 8, pp. 7288–7296, Aug. 2018.

[20] S. Tian, F. C. Lee, Q. Li, and Y. Yan, "Unified equivalent circuit model of v^2 control," in *Proc. IEEE Appl. Power Electron. Conf. Expo.*, 2014, pp. 1016–1023.

[21] S. Tian, F. C. Lee, J. Li, Q. Li, and P. Liu, "A three-terminal switch model of constant on-time current mode with external ramp compensation," *IEEE Trans. Power Electron.*, vol. 31, no. 10, pp. 7311–7319, Oct. 2016.

[22] S. Tian, F. C. Lee, J. Li, Q. Li, and P. Liu, "Equivalent circuit model of constant on-time current mode control with external ramp compensation," in *Proc. IEEE Energy Convers. Congr. Expo.*, 2014, pp. 3747–3754.

[23] Y. Yan, F. C. Lee, P. Mattavelli, and S. Tian, "Small signal analysis of V^2 control using equivalent circuit model of current mode controls," *IEEE Trans. Power Electron.*, vol. 31, no. 7, pp. 5344–5353, Jul. 2016.

Wen-Chin Liu (Student Member, IEEE) received the B.S. degree in electronic and computer engineering from the National Taiwan University of Science and Technology, Taipei, Taiwan, in 2017, the M.S. degree in electrical engineering from National Taiwan University, Taipei, Taiwan, in 2019. He is currently working toward the Ph.D. degree in electrical and computer engineering with the University of California San Diego, La Jolla, CA, USA.

His research interests include modeling, analysis, and control strategies of DCDC converters for point-of-load applications, high frequency, high-power-density dc–dc converters, PV-battery microgrid systems, and piezoelectric resonator-based DC–DC converters.

Ching-Hsiang Cheng received the B.S. degree from the National Yunlin University of Science and Technology, Yunlin, Taiwan, in 2010 and the M.S. degree from National Tsing Hua University, Hsinchu, Taiwan, in 2012, both in electrical engineering, and the Ph.D. degree with Electrical Engineering Department, National Taiwan University, Taipei, Taiwan, in 2020.

He is currently a Power Design Engineer with Google, Taipei, Taiwan, where he designs power solutions for Google data center products. From 2012 to 2016, he has been an Engineer with System Development Center, Richtek Technology Corporation, Hsinchu, Taiwan, working on system analysis and design of controller for dc–dc and ac–dc converter. His research interests include modeling, analysis, and control of ac–dc and dc–dc power converters, power integrated circuits, smart power management integrated circuits, and thermal evaluation for monolithic power integrated circuits.

Patrick P. Mercier (Senior Member, IEEE) received the B.Sc. degree in electrical and computer engineering from the University of Alberta, Edmonton, AB, Canada, in 2006, and the S.M. and Ph.D. degrees in electrical engineering and computer science from the Massachusetts Institute of Technology, Cambridge, MA, USA, in 2008 and 2012, respectively.

He is currently an Associate Professor in electrical and computer engineering with the University of California San Diego (UCSD), La Jolla, CA, USA, where he is also the Co-Director of the Center for Wearable Sensors. His research interests include the design of energy-efficient microsystems, focusing on the design of RF circuits, power converters, and sensor interfaces for miniaturized systems and biomedical applications.

Dr. Mercier was a recipient of numerous awards, including a Natural Sciences and Engineering Council of Canada (NSERC) Julie Payette fellowship in 2006, NSERC Postgraduate Scholarships in 2007 and 2009, an Intel Ph.D. Fellowship in 2009, the 2009 IEEE International Solid-State Circuits Conference (ISSCC) Jack Kilby Award for Outstanding Student Paper at ISSCC 2010, a Graduate Teaching Award in Electrical and Computer Engineering at UCSD in 2013, the Hellman Fellowship Award in 2014, the Beckman Young Investigator Award in 2015, the DARPA Young Faculty Award in 2015, the UC San Diego Academic Senate Distinguished Teaching Award in 2016, the Biocom Catalyst Award in 2017, the NSF CAREER Award in 2018, a National Academy of Engineering Frontiers of Engineering Lecture in 2019, and the San Diego County Engineering Council Outstanding Engineer Award in 2020. From 2015 to 2017, he was an Associate Editor for the IEEE TRANSACTIONS ON VERY LARGE SCALE INTEGRATION (TVLSI). Since 2013, he has been an Associate Editor for the IEEE TRANSACTIONS ON BIOMEDICAL CIRCUITS AND SYSTEMS (TBIOCAS), and is currently a Member of the ISSCC International Technical Program Committee, the CICC Technical Program Committee, the VLSI Symposium Technical Program Committee, and an Associate Editor for the IEEE Solid-State Circuits Letters. Prof. Mercier was the Co-Editor of Ultra-Low-Power Short Range Radios (Springer, 2015) Power Management Integrated Circuits (CRC Press, 2016), and High-Density Electrocortical Neural Interfaces (Academic Press, 2019).

Chunting Chris Mi (Fellow, IEEE) received the B.S.E.E. and M.S.E.E. degrees from Northwestern Polytechnical University, Xi'an, China, and the Ph.D. degree from the University of Toronto, Toronto, ON, Canada, in 1985, 1988, and 2001, respectively, all in electrical engineering.

He is a Professor and the Chair of electrical and computer engineering and the Director with the Department of Energy (DOE)–funded Graduate Automotive Technology Education (GATE) Center for Electric Drive Transportation, San Diego State University, San Diego, CA, USA. Prior to joining SDSU, he was with the University of Michigan, Dearborn, MI, USA, from 2001 to 2015. His research interests include electric drives, power electronics, electric machines, electrical and hybrid vehicles, wireless power transfer, and power electronics.

Dr. Mi was a recipient of the IEEE PELS Emerging Technology Award in 2019, IEEE Transaction on Power Electronics Best Paper Award, and two IEEE Transaction on Power Electronics Prize Letter Awards. He is a Fellow of both IEEE and SAE.